Chalmers Publication Library

Copyright Notice

©2011 IEEE. Personal use of this material is permitted. However, permission to reprint/republish this material for advertising or promotional purposes or for creating new collective works for resale or redistribution to servers or lists, or to reuse any copyrighted component of this work in other works must be obtained from the IEEE.

Maaskant, R., Ivashina, M., Iupikov, O., Redkina, A., Kasturi, S., Shaubert, D.H. (2011) Analysis of large microstrip-fed tapered slot antenna arrays by combining electrodynamic and quasi-static field models. *IEEE Transactions on Antennas and Propagation*, vol. 59, no. 6, pp. 1798-1807.

http://dx.doi.org/10.1109/TAP.2011.2122213

Analysis of Large Microstrip-Fed Tapered Slot Antenna Arrays by Combining Electrodynamic and Quasi-Static Field Models

R. Maaskant, M. V. Ivashina, O. Iupikov, E. A. Redkina,
S. Kasturi, and D. H. Schaubert, *Fellow, IEEE*

***Abstract*— A reduced-order model for large arrays of microstrip-fed Tapered Slot Antennas (TSAs) is presented. The currents on the antenna conductors are modeled by a relatively small number of physics-based macro-domain basis functions through a technique which is known as the Characteristic Basis Function Method (CBFM). The array is treated as a metal-only structure, while the wideband microstrip feeds are separately modeled using quasi-static circuit models. It is demonstrated that, even though the dielectric-supported feeds are non-shielded and therefore form an integral part of each radiating antenna element, the feeds can be modeled independently from the strongly coupled antenna elements. Validation of the combined antenna-feed model has been carried out through the measurements of several practically realized TSA arrays, among them a $8 \times 7 \times 2$ dual-polarized array. The results demonstrate good agreement over a large scan range, as well as over a wide frequency band. The polarization-discrimination capabilities of the antenna, when operating in phased-array mode, have been analyzed in the context of radio-astronomical applications.**

***Index Terms*— Characteristic basis function method, tapered slot antennas, antenna arrays, method of moments, hybrid modeling techniques, radio astronomy.**

Fig. 1. Dual-polarized array of aluminium TSA elements (*cf.* ref. [4]), which is subjected to a reduced-order modeling approach.

I. Introduction

TAPERED slot antennas are traditionally etched on high-performance dielectrics, particularly because dielectrically loaded TSA arrays demonstrate an increased operational impedance bandwidth [1], and offer a direct means to feed the antenna elements as well. However, dielectric-free TSA arrays are low loss and may represent a more cost-effective technology to manufacture large phased-array antennas, which is of great interest to the development of the next generation radio telescope: the Square Kilometer Array (SKA) [2], [3].

In [4], the design of a dual-polarized TSA array has been described where a dielectric substrate is employed, but only locally, and solely for the purpose of feeding each TSA element (see also Fig. 1). The radiating tapered slots are composed of relatively thick aluminum fins in order to realize a slotline capacitance which closely resembles the capacitance of an equivalent slotline sheet that is printed on a dielectric substrate. Furthermore, the relatively thick metals improve the self-supportiveness of the structure. In the present paper we aim to develop a reduced-order model for these types of microstrip-fed TSA arrays.

An accurate full-wave analysis of electrically large TSA arrays is a challenging task, in particular when the strongly coupled wideband antenna elements are composed of both dielectrics and metals of finite geometrical dimensions [5]–[8]. The computational burden of the entire problem can often be relaxed by decomposing it into smaller subproblems that each can be solved relatively easily, and can afterwards be combined into a single aggregated model to obtain its full solution. By decomposing the problem into subproblems, not only the elementary physics of the problem gets revealed, but also the opportunity is offered to perform global optimizations in a time-efficient manner, namely, by first solving for a local subproblem and then accounting for the interactions with its environment, rather than recomputing the entire problem in full detail during each optimization cycle.

In [9], a decomposition technique has been proposed to model the scan impedance of an infinite array of stripline-fed

Manuscript received ?? ??, 20??; revised ?? ??, 20??.

This work is supported by the European Community Framework Programme 6, Square Kilometre Array Design Studies (SKADS), contract no 011938.

R. Maaskant and M. V. Ivashina are with the Netherlands Institute for Radio Astronomy (ASTRON), P.O. Box 2, 7990 AA Dwingeloo, The Netherlands (maaskant@astron.nl; ivashina@astron.nl).

E. A. Redkina and O. Iupikov are with the Sevastopol State Technical University, Radio Engineering Dept., Streletskaya balka, Studgorodok, Sevastopol, 99053, Ukraine (veledle@list.ru, lichne@gmail.com).

S. Kasturi and D. H. Schaubert are with the University of Massachusetts, ECE Department, 215L Marcus Hall, 100 Natural Resources Rd., Amherst MA 01003-9284, USA (skasturi@ieee.org; schaubert@ecs.umass.edu). S. Kasturi is now with Qualcomm in San Diego, California.

TSAs. To model these bilateral structures, a moment-method formulation was proposed based upon the periodic Green's function for currents located inside and on a protruding dielectric slab. The scan impedance was calculated on the stripline feed crossing the slotline section, and therefore included both the reactance of the radial stripline stub, and the stripline-to-slotline transition. The reactance of the stub was independently modeled between two infinite ground planes using the same full-wave formulation. Afterwards, the stub reactance was de-embedded to retain a scan impedance representing only the antenna element and stripline-to-slotline transition. It was concluded that the radial stub can be optimized independently, and be seen as an individual reactance in series with the de-embedded scan impedance representing only the antenna and stripline-to-slotline transition.

A further decomposition into microwave circuit models has been proposed in [10]. Therein, the microstrip-to-slotline transition is modeled by Knorr's equivalent circuit [11] (an ideal transformer), whereas the microstrip stub and feed lines, and even the slotline cavity of the antenna, have all been modeled by ideal transmission lines. Following this, it has been demonstrated in [12] that both the microstrip feed and antenna slot cavity of a single bunny-ear antenna can then be optimized to realize a desired impedance bandwidth. However, in [9], it has been stated that, for arrays of TSAs, both the tapered slot and the slotline cavity exhibit a significant interaction with the neighboring elements. As a result, a quantitative analysis of wideband phased arrays was not found to work for such a detailed antenna-feed decomposition.

In this paper, it is explained how the feed model can be modified in order to analyze (large) arrays of TSAs in a quantitative manner. The distinction with other papers is that both the strongly coupled tapered slots and the slotline cavities are now represented by electrodynamic field models, whereas the microstrip lines and stubs, including their microstrip-to-slotline transitions, are represented by quasi-static field models. The antenna array can be analyzed as a dielectric-free structure if the effect of the dielectric substrate on its radiation characteristics is negligible, which is particularly true if the dielectric: (i) is employed only locally; (ii) is effectively thin compared to the TSA fins, and; (iii) has a low relative dielectric permittivity. We will consider only one specific realization for which mainly the first two requirements are satisfied.

The dielectric-free antenna array is analyzed with the aid of the moment method in which we employ an adequate number of numerically generated entire-domain basis functions on each of the metallic TSA elements and then account for the mutual reaction between them through the Characteristic Basis Function Method (CBFM) [13]. The direct interaction between antenna feed boards is neglected as the coupling is assumed to occur only via antenna elements.

Validation of the impedance characteristics of the combined quasi-static and electrodynamic field models has been carried out via measurements for several practically realized TSA arrays. The results demonstrate a very good agreement over a large scan range, as well as over a wide frequency band.

II. Geometrical Dimensions of the Reference TSA

Fig. 2(a) illustrates the geometrical dimensions of the reference TSA element that has been examined. The element geometry has been adopted from [4], where the design of an infinite dual-polarized phased array of such elements has been described and analyzed with the aid of periodic boundary conditions.

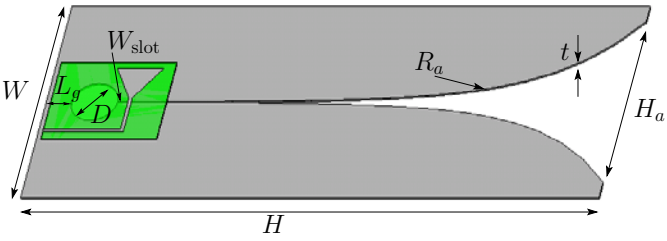

W	L_{g}	D	W_{slot}	H	R_{a} (cm^{-1})	t	H_{a}
12.5	1.3	2.4	0.05	30	0.25	0.1	10.5

(a)

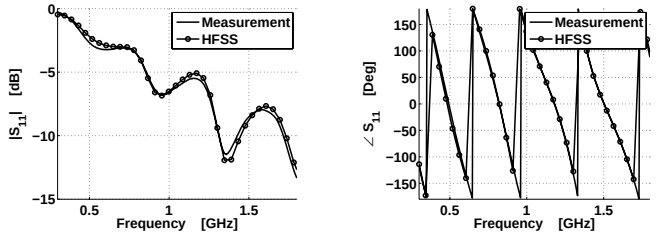

(b) (c)

Fig. 2. (a) Geometrical dimensions of the reference TSA element in cm. The magnitude and phase of S_{11}, both measured and simulated, are shown in figures (b) and (c), respectively.

The magnitude and phase of S_{11} of a single array element, both measured and simulated, are shown in Figs. 2(b) and 2(c), respectively. The agreement between the measured and simulated (HFSS) impedance characteristics of a single TSA element (mounted on an infinitely large PEC ground plane) is sufficiently good and will, henceforth, be used in the development and validation of the combined model for both the microstrip feed and the antenna structure.

III. Reduced Order Model of a Single Microstrip-fed TSA

We will utilize the measurements or simulations of a single TSA element to extract the model parameters of the microstrip feed. First, the TSA element is excited by a voltage-gap generator across the slotline section in the absence of the microstrip feed. The currents inside the actual antenna conductor of finite thickness are effectively represented by average surface currents supported by infinitely thin metallic sheets. It is crucial that the actual thickness of the conductors is modeled accurately in order to obtain the correct fields inside the slot region, and thereby the correct gap impedance. Therefore; the edges of the current sheets have been right-angled folded as illustrated in Fig. 3.

Next, the current sheets are supplied with a triangular mesh (see Fig. 3) and an adequate number of subsectional Rao-Wilton-Glisson (RWG, [14]) basis/testing functions is

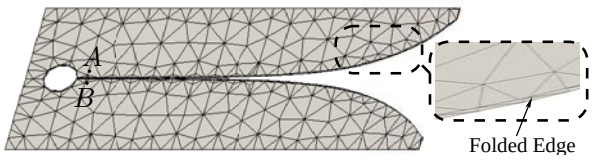

Fig. 3. Triangular meshed TSA element with folded edges to simulate a finite thickness of the metal, and delta-gap excitation between A and B.

employed. The surface current is subsequently synthesized by discretizing an Electric Field Integral Equation (EFIE) with the aid of the moment method (Galerkin's testing scheme), after which the resulting system of linear equations is solved for the unknown RWG expansion coefficients.

After computing the antenna impedance between terminals A–B (see Fig. 3), the microstrip feed is modeled as schematically shown in Fig. 4.

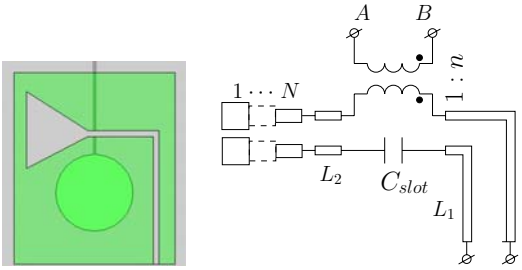

Fig. 4. (a) A microstrip feed on a localized substrate carrier, and; (b) an equivalent circuit representation of this feed. Preliminary results have been reported for a 3×1 TSA array in [15].

Fig. 4(b) illustrates a modified representation of Knorr's equivalent circuit [11] in which the microstrip-to-slotline transition is modeled as an ideal transformer with a (non-integer) turns ratio $n = V_{\rm sec}/V_{\rm prim}$, where $V_{\rm prim}$ and $V_{\rm sec}$ are the microstrip and slotline voltages across the primary and secondary windings, respectively. A capacitor has been added in series with the microstrip line because the ground conductor of the microstrip line is interrupted by the slotline. We therefore have placed this capacitor in the ground conductor of the transformer [*cf.* the actual situation in Fig. 4(a)]. This capacitor becomes a required element when wide slots and low-permittivity substrates are considered. However, in the present case the slot is relatively narrow and composed of two relatively thick metals, so that the capacitor becomes virtually short-circuited and therefore a non-required circuit element.

As described in [16], the impedance of wide-band circular stubs can be accurately modeled by a cascaded series of transmission lines with varying strip widths, although this method neglects the stub radiation, parasitic effects at junctions, and the fringing field effect at the stub end. Because the latter effects are small, also the impedance of the triangular stub of Fig. 4(a) could be accurately modeled with this technique. For this purpose, the design equations of [17, pp. 87–92] for each of the microstrip sections were used, and the stub impedance was evaluated for a series of cascaded sections with the help of the CAESAR circuit simulation software [18].

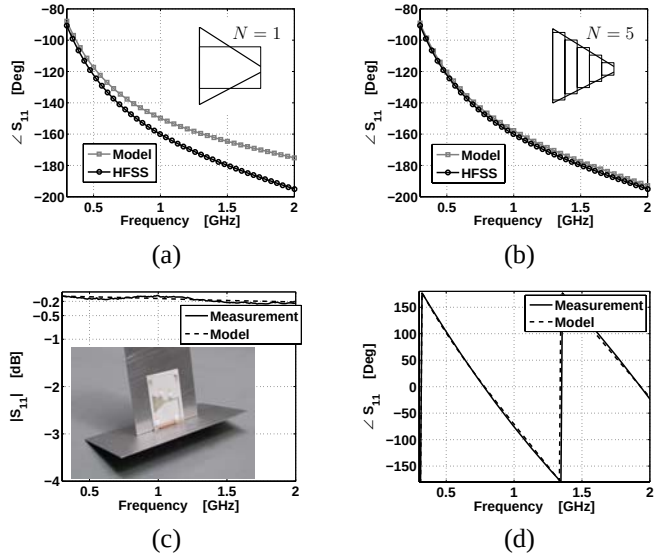

Fig. 5. The modeled and simulated (HFSS) phase of S_{11} of the (a) triangular stub ($Z_{\rm ref} = 50\Omega$) using (a) $N = 1$ section; (b) $N = 5$ sections. (c), (d) The measured magnitude and phase of the reflection coefficient of the microstrip-feed section (transformer short circuited).

The impedance of the triangular stub has also been computed with the aid of a full-wave method (HFSS) and subsequently compared to the presently modeled stub impedance; the results are shown in Fig. 5. The phase accuracy of the reflection coefficient is even reasonable for a single microstrip section, but readily improves by adding a few more sections. The magnitude of the reflection coefficient of the stub only is not shown since $|S_{11}| > -0.05$ dB for both models over the entire frequency band. The reflection coefficient of the entire microstrip feed section, when placed above a PEC ground plane (transformer short circuited), has both been measured and simulated. The agreement for the magnitude in Fig. 5(c), and phase in Fig. 5(d) is very good, even outside the operational frequency range from 0.5–1.5 GHz. Because the microwave network is non-radiative, the dissipation losses are only due to the ohmic losses in the conductor and the dielectric material. For the computations, we have used that $\tan(\delta) = 0.0027$ and $\sigma_{\rm cond} = 5.8 \times 10^7\ \Omega^{-1}{\rm m}^{-1}$. The corresponding frequency-dependent attenuation coefficients $\alpha_{\rm diel}$ and $\alpha_{\rm cond}$, for a passively-matched terminated microstrip line, range from $0.01-0.1$ Np/m and $0.03-0.1$ Np/m, respectively. As a result, it is observed in Fig. 5(c) that $|S_{11}| > -0.2$ dB for a standing-wave current along the microstrip feed.

Since the physical dimensions of the microstrip feed as well as the electrical properties of the substrate carrier are known ($\varepsilon_r = 3.38$, $d_{\rm sub} = 0.8$ mm, $w_{\rm strip} = 1.8$ mm), most of the model parameters of the equivalent circuit [Fig. 4(b)] can readily be determined, and are listed in Table I.

TABLE I
MODEL PARAMETERS OF THE CIRCUIT SHOWN IN FIG. 4

N	L_1	L_2	$Z_{\rm ref}$	n	$C_{\rm slot}$
5	67.8 mm	2.2 mm	50 Ω	0.95	–

The length L_1 of the transmission line includes the equiv-

alent connector length. The parameter n has been determined by a least-squares fit of the port impedance of the cascaded model (antenna+feed) onto the reference impedance shown in Figs. 2(b) and 2(c). Although n is generally a complex-valued quantity, it is herein taken real-valued since the capacitor accounts for a possible reactive part. Moreover, the conservation of power between the primary and secondary windings is then automatically satisfied. We remark that n and C_{slot} need to be determined only once because they solely depend upon the geometry of the microstrip-to-slotline transition, which is often not altered during a design optimization, as opposed to the geometry of the triangular stub, circular cavity, exponential taper, width and height of the TSA element.

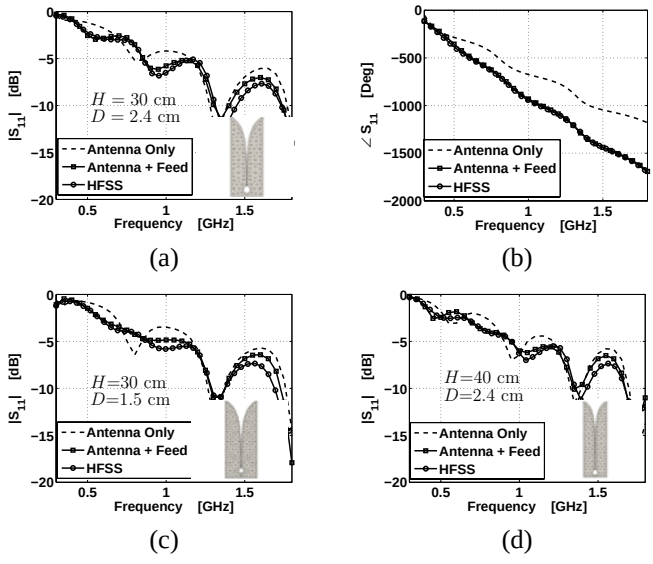

Fig. 6. Modeled and full-wave simulation results (HFSS) of S_{11} of a single TSA element ($Z_{\text{ref}} = 50\Omega$). The magnitude (a) and phase (b) of S_{11} for the reference geometry. (c); (d) The magnitude $|S_{11}|$ for two different element geometries but for identical feed models.

Figs. 6(a) and 6(b) illustrate that the overall return loss of the cascaded antenna in combination with the feed circuit is in good agreement with the reference full-wave solution (HFSS). Figs. 6(c) and 6(d) depict the magnitude of S_{11} when the circular cavity size D and the height H of the TSA element are varied. As expected, the accuracy remains good when the TSA element geometry is altered, while the feed geometry and its model parameters are kept fixed. This confirms that n is almost invariant to these geometrical changes. The S_{11} of the antenna element in the absence of the feed circuit is also shown for these cases, and illustrates that the effect of the feed circuit on the return loss is rather significant.

The HFSS v10 computations have been performed on a Linux desktop PC which has 8 GB of RAM and 2 dual core AMD processors.

IV. Analysis of Large TSA Arrays

It is important to demonstrate that the non-radiative feed model, which has been developed for a single TSA element, can directly be applied to analyze the impedance characteristics of large arrays of mutually coupled TSAs. In this paper, we showcase some specific results of CBFM for a 4×4 singly-polarized and an 8×7 doubly-polarized TSA array.

The antenna impedance matrix of a large antenna array can be computed using a recently introduced enhancement technique for the moment method, known as the Characteristic Basis Function Method (CBFM) [19]. In CBFM, a large problem is reduced to a manageable size by using a domain decomposition technique; it derives a reduced matrix, which preserves all of the coupling effects rigorously when it is formed, and subsequently solves the resultant matrix equation in a direct manner instead of resorting to iteration algorithms to handle the problem of interaction between the various subdomains. Details on CBFM, the generation of the physics-based macro domain basis function (CBFs), and its extensions can be found in a number of papers, among these [13], [21], [22], and references therein. The concept of reducing the matrix equation and decomposing the problem into smaller problems has also been exploited in other iterative-free methods for large-scale problems. Examples are: the Synthetic-Functions Approach (SFX) [23], [24]; the Sub-Entire-Domain basis function method (SED) [25]; the eigencurrent approach [26]; the multipole macro basis function approach [27]; and a subdomain multilevel approach [28].

The CBFM computations have been carried out in double precision arithmetic on a Dell Inspiron 9300 Notebook, equipped with an Intel Pentium-M processor operating at 1.73 GHz, and 2.0 GB of RAM. To achieve high solution accuracy, the threshold of the singular value decomposition (SVD), which is used to orthonormalize and to truncate the number of numerically generated CBFs, has been set to 10^{-4}. The threshold of the Adaptive Cross Approximation (ACA) algorithm, which is used for the fast construction of off-diagonal (reduced) moment matrix blocks, has been set to 10^{-3} [13].

For antenna problems, it is customary to generate and employ primary and secondary CBFs [13]. However, we will illustrate that, from an accuracy point of view, one can supplement or even obviate the generation of secondary CBFs and, equally well, let a spectrum of incident plane waves (PWS) be incident on a smaller subarray. These additional CBFs are needed to accurately synthesize the coupling effects for TSA elements farther out, and are appended to the already existing set of primary CBFs (after applying a trapezoidal post-windowing procedure, [20]). For this purpose, a PWS is used for the two orthogonal theta and phi polarizations with an angular step size of 20^o (typical value) in both the theta and phi directions, where the theta range is limited to the upper hemisphere in case an infinite ground plane is present.

A. Results for a 4×4 Singly-Polarized TSA Array

To be able to validate the measured antenna impedances by commercial solvers, a relatively small 4×4 singly-polarized TSA array has been fabricated as shown in Fig. 7(a). Although the problem requires only 9848 RWG basis functions, it cannot be handled by a plain MoM solver because of memory overflow errors above $\sim$ 7000 RWGs. When CBFM is used instead, it is worth realizing that the computational overhead

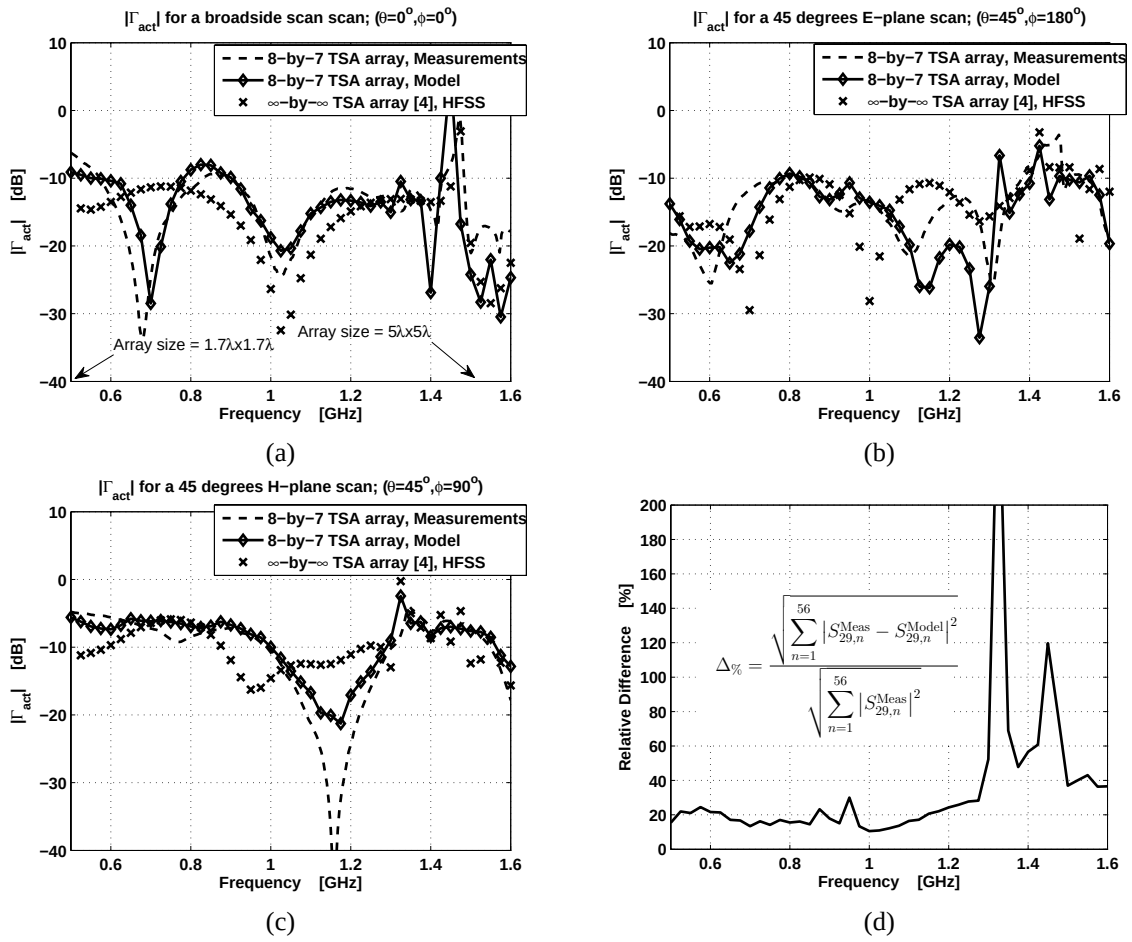

Fig. 8. (a)–(c) Magnitude of the measured and simulated active scan reflection coefficient Γ_{act} of a center element as a function of frequency and for various scan directions. The HFFS results are for an $\infty \times \infty$ TSA array [4]. (d) The relative difference of the measured and simulated coupling between the center element and all other equally polarized elements as a function of frequency.

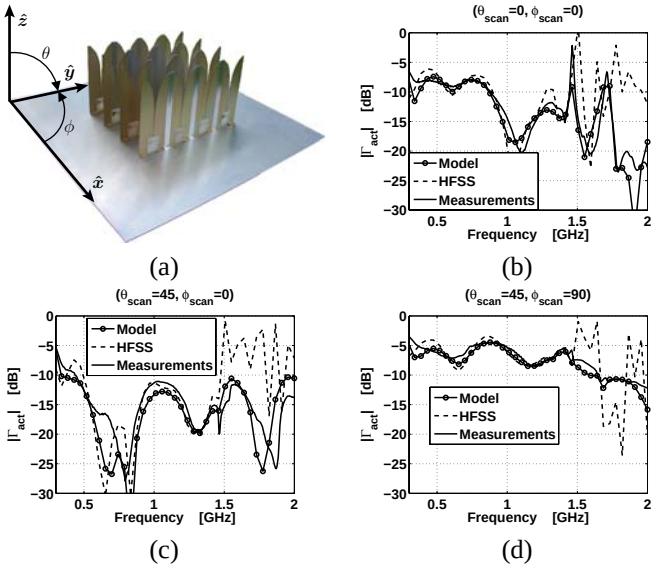

Fig. 7. (a) A 4×4 singly-polarized microstrip-fed TSA array mounted on a finite ground plane. The magnitude of the measured, simulated (HFSS), and modeled active scan reflection coefficients are shown for: (b) $\theta = 0^\circ$, $\phi = 0^\circ$; (c) $\theta = 45^\circ$, $\phi = 0^\circ$ (H-plane scan), and; (d) $\theta = 45^\circ$, $\phi = 90^\circ$ (E-plane scan).

of CBFM is relatively large for small arrays, since the total execution time (for this case ~ 1 hour per frequency point) is governed by the time to generate CBFs and to construct a reduced matrix. The details on CBFM will therefore only be discussed for the larger 8×7 dual-polarized TSA array for which it outperforms any direct moment method solver, hypothetically.

From the measured antenna S-parameters, we have computed the active scan reflection coefficient Γ_{act}^n for the nth antenna element as

$$\Gamma_{\text{act}}^n = \frac{1}{a_n} \sum_{m=1}^{N} S_{nm} a_m \tag{1}$$

where a_p for $p \in \{m, n\}$ is the complex amplitude of the excitation wave incident on the pth antenna port with $p \in \{1, 2, \ldots, N\}$.

Figs. 7(b)–(d) depict the active scan reflection coefficients of one of the four center elements for different phased-array excitation schemes. A good agreement is observed between the measured and modeled magnitudes of the active reflection coefficients for various scan angles and as a function of frequency. The results that have been computed by the finite element solver HFSS are also in good agreement, i.e., up to $\sim$ 1.5 GHz. The high-frequency results ($\gtrsim$ 1.5 GHz) have

been computed with reduced accuracy because of memory constraints. More specifically, to assure that the size of the radiation box is $\lambda/4$ away from element edges at 0.5 GHz, the solution frequency for convergence (used for adaptive mesh refinement in HFSS) had to be set to 1.0 GHz (the center frequency). Finally, it is worth mentioning that the onset of grating lobes above 1.2 GHz occurs in conjunction with high-Q impedance resonances which are difficult to predict accurately with limited computational resources.

B. Results for an 8×7 Doubly Polarized TSA Array

The impedance matrix of the 112-port TSA array of Fig. 1 has been evaluated for the above proposed model and compared to measurements. The problem requires 79450 RWG basis functions, which is a degree-of-freedom that would significantly increase whenever the dielectric microstrip feed becomes part of the EM model, and such a problem is beyond the reach of (most) commercial solvers.

The first step in solving this problem is to construct the entire array mesh. We mesh only two base elements (a co- and cross-polarized antenna element) and the bottom edge of each base element is connected along the diagonal of a square ground plane. Note that, when such a base element is replicated at the various element positions throughout the lattice, a finite dual-polarized array is formed over a finite ground plane.

After the construction of the entire array mesh, a minimum number of unique supports[1] is identified throughout the array lattice each of which holds a distinct set of CBFs. Any other support function (associated to an array element), inherits one of these unique sets of CBFs through translation. In the end, all the array elements support a set of (mutually overlapping) CBFs. The total number of identifiable unique sets of CBFs depends on the regularity of the meshed antenna array geometry and is independent of the array size [29]. For the present problem we generate 18 sets of CBFs by extracting 18 subarrays from the fully meshed array. That is, for each polarization, we extract 4 corner element, 4 edge elements, and an inner element along with their direct electrically interconnected adjacent elements. Next, currents are induced on these 18 subarrays by exciting each of the array elements sequentially as well as by applying a PWS, after which the supports of these currents are reduced to the size of a single element plus a minor extension [20]. The 18 sets of CBFs generated in this manner are subsequently mapped onto the array mesh through translation. Finally, each of the 112 antenna elements supports a set of CBFs which partially overlaps with the CBFs supported on the electrically interconnected adjacent elements, and this preserves the continuity of the current in the final solution. By using a 20 degrees angular step size of the PWS, and a SVD threshold of 10^{-4}, about 31 CBFs are generated for each of the 112 antenna elements (@ 1.0 GHz).

[1]In the present overlapping domain-decomposition technique, a CBF support is comprised of the mesh of one antenna element including a minor extension over the electrically interconnected adjacent elements.

The above meshing strategy has been detailed in [29] and allows for a fast construction of the (reduced) moment matrix since we can exploit the block-Toeplitz symmetry of this matrix. This is possible since a large degree of translation symmetry exists between group pairs of RWGs (or CBFs) throughout the array lattice. Because of this symmetry, only 5166 unique moment matrix blocks out of the $112 \times 112 = 12544$ need to be constructed to compute the reaction integrals between CBFs (reciprocity not exploited).

The reduced matrix equation is solved through Gaussian elimination for 112 excitation vectors (112 element excitations). The total execution time, which also includes the meshing and post-processing time of the currents, impedances, far-field patterns, and the solve time of the microwave network, is shown in Table II.

TABLE II
TOTAL EXECUTION TIME (@ 1.0 GHZ, FOR 79450 RWGS).

CBF generation for 18 distinct supports in the array	1 h. 51 min.
Construction of the reduced matrix equation	0 h. 50 min.
Computation of CBF far-field patterns (18 sets)	0 h. 45 min.
Total number of CBFs	3506
Solve time reduced matrix equation (3506×3506)	36 sec.
Total execution time	3 h. 36 min.

The magnitude of the measured and simulated active scan reflection coefficient Γ_{act} for a center element as a function of frequency is shown in Figs. 8(a)–(c). For completeness, the HFSS results for a periodic unit-cell analysis of an infinite-by-infinite TSA array have been overlayed with the finite array results. Even though the array size is only $5\lambda \times 5\lambda$ at 1.5 GHz, the active impedance characteristics are comparable for a broadside scan down to 0.8 GHz. Deviations are mainly caused by edge-truncation effects, which increase at low frequencies and large scan angles. Three scan angles have been considered: broadside scan ($\theta = 0^o, \phi = 0^o$), a 45 degree E-plane scan ($\theta = 45^o, \phi = 180^o$), and a 45 degree H-plane scan ($\theta = 45^o, \phi = 90^o$). Only the x-oriented TSAs are excited, while the cross-polarized elements are passively terminated by 50 Ohm loads at the microstrip feed ends. Even though the proposed antenna-feed decomposition approach is rather approximate, the agreement between measurements and simulations is found to be remarkably good. In fact, up to the first resonance frequency, at around 1.45 GHz (broadside scan), the relative difference between the measured and modeled mutual coupling coefficients between the center element (#29) and all other equally polarized elements, is about 20%. This result has been plotted in Fig. 8(d). The resonance seems well-predicted in Fig. 8(a); however, it is obvious that the relative difference as defined in Fig. 8(d) can become large $(> 100\%)$ due to a minor frequency shift.

Fig. 9 visualizes the measured and simulated magnitudes and phases of the coupling coefficients between the center element (#29) and all other equally polarized elements (@ 1.0 GHz). It is observed from the contour plots in Fig. 9(c) and (d) that the E-plane coupling is stronger than the H-plane coupling, but this depends on frequency and the reference impedance (element termination). The latter can also

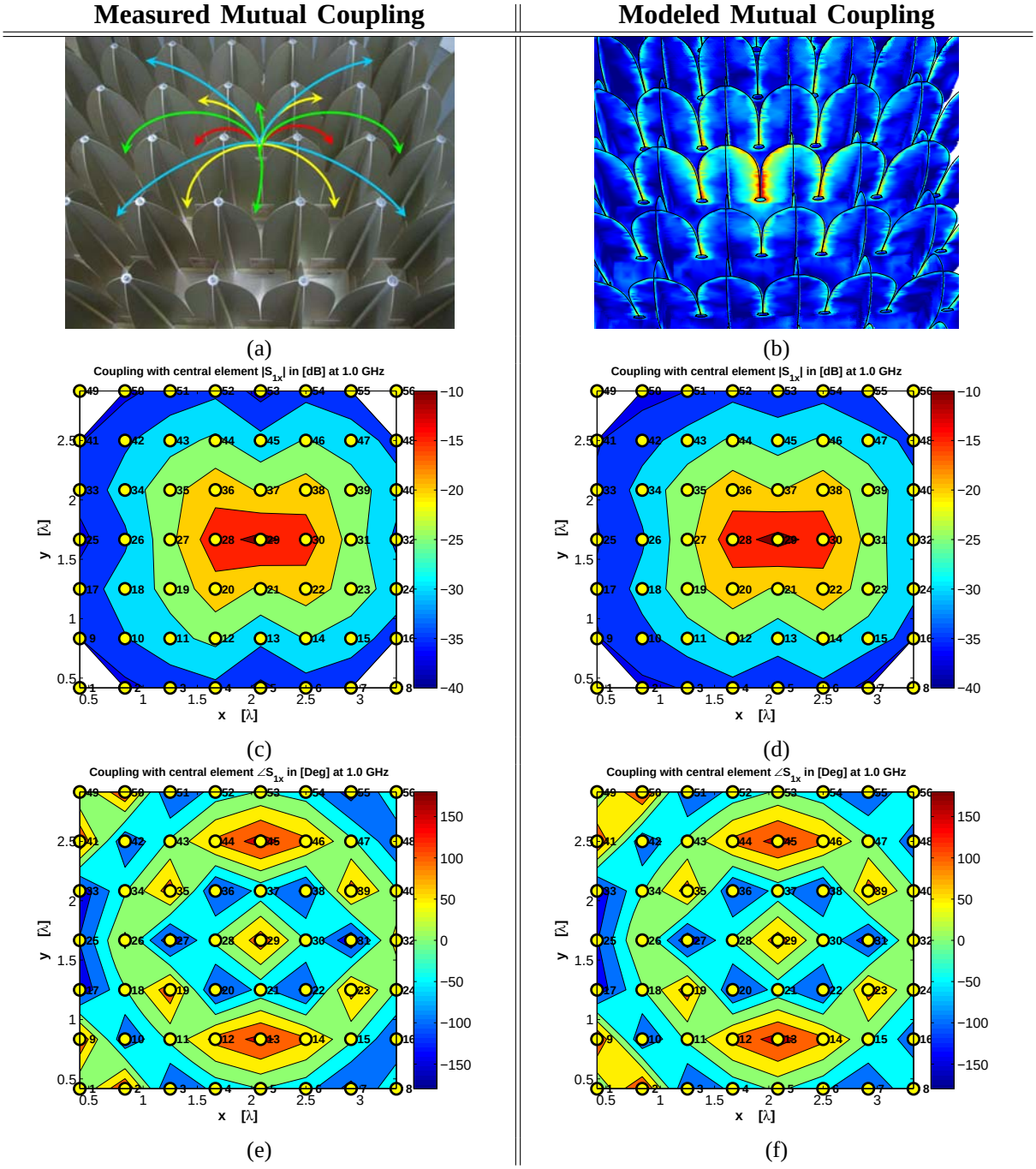

Fig. 9. Results for the measured and simulated mutual couplings $S_{29,x}$ for $x = 1, \ldots, 56$, between the central element $x = 29$ and all other equally polarized elements, for 1.0 GHz. (a) Top view of the array. (b) Magnitude of the current when element 29 is excited (logarithmic scale, 60 dB dynamic range). (c) The measured $|S_{29,x}|$ in dB. (d) The simulated $|S_{29,x}|$ in dB. (e) The measured $\angle S_{29,x}$ in Deg. (f) The simulated $\angle S_{29,x}$ in Deg.

be concluded from the magnitude of the current distribution shown in Fig. 9(b). Both the magnitude and phase distributions are well predicted, that is, the relative difference according to Fig. 8(d) is $\sim 10\%$ @ 1.0 GHz. A similar agreement is obtained at other frequencies, except near or above 1.3 GHz, where element impedances are disrupted by resonant array effects which are difficult to predict accurately (the $\lambda/2$ element separation distance is at 1.2 GHz). In this respect, it is also worth mentioning that the microstrip feed boards have been glued on the elements by hand, and that, due to this, the relative spread (standard deviation of S_{11} divided by its mean value) in measured impedances between four isolated elements can be as large as 25% in the frequency band of operation. This variation is partly caused by a misalignment of the feed, and/or a small air gap between the microstrip feed board and the aluminium antenna. Measurements with a Time Domain Reflectometer revealed that, for each μm air gap, the characteristic impedance of the microstrip line increases by 72 mΩ. The maximum in relative spread occurs at 900 MHz, and this is also observed in Fig. 8(d). It is likely that an increase in the relative difference between the modeled and simulated coupling coefficients in Fig. 8(d) is partly due to

fabrication tolerances. Mechanically more robust solutions to firmly clamp the feed are currently being examined [30].

Even though element #29 is not an exact center element, one expects symmetry in the computed coupling coefficients along the y-direction. The coupling coefficients are derived from the moment matrix solution, but from the reaction concept and reciprocity theorem, we know that symmetry is preserved in the moment matrix whenever Galerkin's method is combined with a symmetric product for testing the integral equation. However, in our implementation, the moment matrix is only symmetric for a limited number of computed digits because the source and test integrals are evaluated using unequal quadrature rules. The relative error in the computed matrix elements is typically smaller than the $\sim$ -30 dB level with respect to the largest computed ones. The degree of asymmetry depends on the mutual orientation between pairs of RWGs and the order of the Gaussian quadrature rule that is employed to compute their reaction integrals (i.e. the moment matrix entries). If desired, the degree of symmetry can be improved by choosing equal quadrature rules or by increasing their orders at the cost of a reduced matrix-fill time. Also, we found that the symmetry improves by lowering the ACA threshold level. Reciprocity can be exploited beyond a certain point and would save approximately a factor of two in total fill-time.

V. Simulated Far-Field Patterns and Orthogonality of a Co- and Cross-Polarized Array Beam

The computed embedded-element patterns are illustrated in Fig. 10. These are the patterns that arise if one element is excited, while the other elements are passively-matched terminated using 50 Ohm loads at the microstrip feed ends. Due to edge-truncation effects, the far-field patterns of the

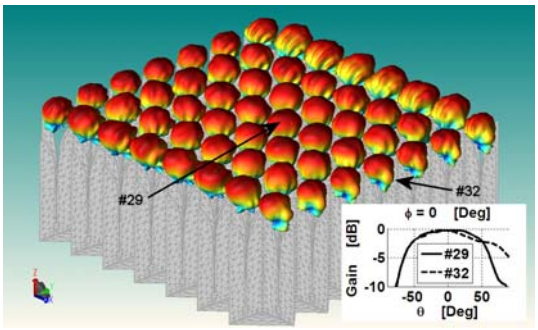

Fig. 10. Embedded-element power-patterns at 1.0 GHz (linear scale).

edge and corner elements exhibit many ripples and, although not shown, were found to be frequency-dependent as well. Furthermore, as a result of the coupling effects, it can be observed that the power patterns of the center elements are "smoother" and more symmetrical than the patterns of the boundary elements.

In radio astronomy, it is of primary importance to recover the intensity and/or polarization information of the incident electromagnetic field radiated by a (partially polarized) source in the sky (the Stokes parameters [31, p. 4-8]). To measure these Stokes parameters, we can let the 112 TSA element array operate in phased-array mode and separately combine the output signals of the x- and y-oriented elements into a co- and cross-polarized beam, respectively. Even though the pertaining array elements are geometrically orthogonal to each other, it is essential that also the realized co- and cross-polarized beams are sufficiently orthogonal over a large scan volume and frequency band in order to effectively recover the Stokes parameters of the incident field [32].

Let the vectors

$$\boldsymbol{e}^{\text{co}}(\theta_0,\phi_0) = e^{\text{co}}_\theta \hat{\boldsymbol{\theta}} + e^{\text{co}}_\phi \hat{\boldsymbol{\phi}} \tag{2a}$$

$$\boldsymbol{e}^{\text{cross}}(\theta_0,\phi_0) = e^{\text{cross}}_\theta \hat{\boldsymbol{\theta}} + e^{\text{cross}}_\phi \hat{\boldsymbol{\phi}} \tag{2b}$$

denote the complex-valued electric far-field vectors of the realized co- and cross-polarized beam patterns in the direction (θ_0,ϕ_0) of the source. These vectors are normalized such that $V_x = \boldsymbol{e}^{\text{co}} \cdot \boldsymbol{E}^i$ and $V_y = \boldsymbol{e}^{\text{cross}} \cdot \boldsymbol{E}^i$ are the received output voltages corresponding to the x- and y-oriented elements, respectively. Clearly, the set $\{\boldsymbol{e}^{\text{co}}, \boldsymbol{e}^{\text{cross}}\}$ forms a basis along which the incident field $\boldsymbol{E}^i$ is decomposed. The beam orthogonality in the (θ_0,ϕ_0) direction is conveniently measured through the normalized cross-correlation term

$$\rho_{\text{cor}} = \frac{\langle \boldsymbol{e}^{\text{co}}, \boldsymbol{e}^{\text{cross}} \rangle}{\sqrt{\langle \boldsymbol{e}^{\text{co}}, \boldsymbol{e}^{\text{co}} \rangle \langle \boldsymbol{e}^{\text{cross}}, \boldsymbol{e}^{\text{cross}} \rangle}} \tag{3}$$

where $\langle \boldsymbol{a}, \boldsymbol{b} \rangle = \boldsymbol{a}^* \cdot \boldsymbol{b} = \boldsymbol{a}^H \boldsymbol{b}$ represents the Hermitian inner product. We point out that, if $\rho_{\text{cor}}(\theta_0,\phi_0) = 0$, the beams are orthogonal in the (θ_0,ϕ_0) direction and the Stokes parameters can, potentially, be measured with high precision, provided that a possible rotation of this orthogonal basis with respect to a given reference frame (usually of the source) is known and can be corrected for in the post-processing of the data (calibration). On the contrary, if $|\rho_{\text{cor}}(\theta_0,\phi_0)| \approx 1$, the Stokes parameters can be recovered with low precision. One could orthonormalize this basis by adapting the beamformer weights, but this is likely to result in a loss of sensitivity as well.

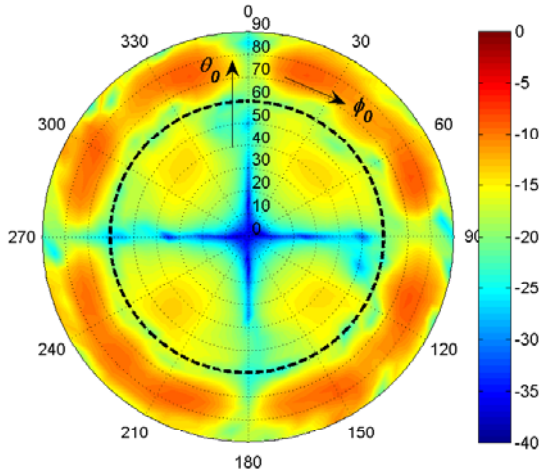

Fig. 11. Correlation (here used as the measure of orthogonality) between a co- and cross-polarized beam in the scan direction (θ_0,ϕ_0), for $0 \le \theta_0 \le 90^o$ and $0 \le \phi_0 \le 360^o$. The scale is logarithmic.

The beam orthogonality $10\log(|\rho_{\text{cor}}|)$ of the 112 TSA element array has been analyzed over a large scan volume

(@ 1.0 GHz). The results are shown in Fig. 11. As expected, the orthogonality is best in the principle planes, i.e., in the E and H planes, but ρ_{cor} reduces in the D planes down to -14 dB for $0 \leq \theta_0 \leq 60^o$. The level of orthogonality that is required depends on the kind of observation and the operation of the system as a whole; it is therefore considered to be a system specification, even though the beam orthogonality as presented in Fig. 11 is rather intrinsic to the antenna type, excitation scheme, and the chosen array configuration. Also, it should be clear that, to some extent, the co and cross polarization of a single TSA element may not be very important; it is the combination of the patterns generated by x- and y-oriented antennas which realizes the beam pair determining the capabilities of the instrument to perform an adequate polarization discrimination.

VI. Conclusions

We have shown that it is feasible to analyze mutual coupling effects in large microstrip-fed TSA arrays by using a combination of an electromagnetic and a quasi-static field model of the antenna and feed, respectively. The relative difference between the measured and simulated coupling coefficients of a 8×7 dual-polarized TSA array is $\sim 20\%$ over the operational frequency band, which is comparable to the manufacturing tolerances of the TSAs. Although the array is relatively small, impedance anomalies appear in the measurements as well as in the finite-array simulations. Since TSA arrays are strong candidates for the next generation radio telescopes, we have also examined the polarization-discrimination capabilities of a phased-array aperture tile over the entire scan volume. The correlation (here used as the measure of orthogonality) between a transmitted pair of E-field vectors into a certain scan direction, each of which is generated by exciting either the co- or cross-polarized array elements, was found to be better than -14 dB for $0 \leq \theta \leq 60^o$.

References

[1] S. Kasturi and D. H. Schaubert, "Effect of dielectric permittivity on infinite arrays of single-polarized Vivaldi antennas," *IEEE Trans. on Antennas and Propagat.*, vol. 54, no. 2, pp. 351–358, Feb. 2006.

[2] P. J. Hall, "The square kilometre array: an engineering perspective" Reprinted from experimental astronomy, vol. 17, no. 1–3, 2004, ISBN: 1-4020-3797-x, Springer 2005.

[3] A. B. Smolders and M. P. van Haarlem, "Perspectives on radio astronomy: technologies for large antenna arrays," Conf. Proc., ASTRON, ISBN: 90-805434-2-x, April 1999.

[4] R. Maaskant, M. Popova, and R. van de Brink, "Towards the design of a low cost wideband demonstrator tile for the SKA," *Proc. European Conf. on Antennas and Propagat.*, Nice, France, 2006.

[5] W. Yu, X. Yang, Y. Liu, L.-C. Ma, T. Su, N.-T. Huang, R. Mittra, R. Maaskant, Y. Lu, Q. Che, R. Lu, and Z. Su, "A new direction in computational electromagnetics: solving large problems using the parallel FDTD on the BlueGene/L supercomputer providing teraflop-level performance," *Antennas and Propagat. Magazine*, vol. 50, no. 2, April 2008, pp. 26–44.

[6] M. N. Vouvakis, S.-C. Lee, K. Zhao, and J.-F. Lee, "A symmetric FEM-IE formulation with a single-level IE-QR algorithm for solving electromagnetic radiation and scattering problems," *IEEE Trans. on Antennas and Propagat.*, vol. 52, no. 11, pp. 3060–3070, Nov. 2004.

[7] C. Craeye, and X. Dardenne, "Fast numerical analysis of finite arrays of antennas in finite dielectric volumes," *Proc. ICEAA Conf.*, Torino, Italy, Sep. 17-21, 2007.

[8] L. Matekovits, G. Vecchi, M. Bercigli, and M. Bandinelli, "Synthetic-functions analysis of large aperture-coupled antennas," *IEEE Trans. on Antennas and Propagat.*, vol. 57, no. 7, pp. 1936–1943, July 2009.

[9] J. Shin and D. H. Schaubert, "A parameter study of stripline-fed Vivaldi notch-antenna arrays," *IEEE Trans. on Antennas and Propagat.*, vol. 47, no. 5, pp. 879–886, May 1999.

[10] D. H. Schaubert, "Endfire slotline antennas," *JINA conf.*, Journees internationals de Nice sur les Antennes, Nice, France, pp. 253–265, Nov. 1990.

[11] J. B. Knorr, "Slotline Transitions," *IEEE Trans. Microwave theory Tech.*, vol. MTT-22, pp. 548–554, 1974.

[12] A. B. Smolders and M. J. Arts, "Wide-band antenna element with integrated balun," *IEEE AP-S International Symposium*, Atlanta, USA, pp. 1394–1397, 1998.

[13] R. Maaskant, R. Mittra, and A. G. Tijhuis, "Fast analysis of large antenna arrays using the Characteristic Basis Function Method and the Adaptive Cross Approximation Algorithm," *IEEE Trans. on Antennas and Propagat.*, vol. 56, no. 11, pp. 3440–3451, Nov. 2008.

[14] S. Rao, D. Wilton, and A. Glisson, "Electromagnetic scattering by surfaces of arbitrary shape", *IEEE Trans. Antennas Propag.*, vol. 30, no. 3, pp. 409–418, May 1982.

[15] M. V. Ivashina, E. A. Redkina, and R. Maaskant, "An accurate model of a wide-band microstrip feed for slot antenna arrays," *IEEE AP-S International Symposium*, Hawaii, USA, pp. 1953–1956, 2007.

[16] B. Schüppert, "Microstrip-slotline transitions: modeling and experimental investigation," *IEEE Trans. Microwave Theory Tech.*, vol. 36, pp. 1272–1282, 1988.

[17] K. C. Gupta, R. Garg, and I. Bahl, "Microstrip lines and slotlines," *Artech House*, Norwood, MA, 1979.

[18] R. Maaskant and B. Yang, "A combined electromagnetic and microwave antenna system simulator for radio astronomy," *Proc. European Conf. on Antennas and Propagat.*, Nice, France, 2006.

[19] J. Yeo, V. Prakash, and R. Mittra, "Efficient analysis of a class of microstrip antennas using the Characteristic Basis Function Method (CBFM)", *Micr. Opt. Technol.* vol. 39, pp. 456–464, Dec. 2003.

[20] R. Maaskant, R. Mittra, and A. G. Tijhuis, "Application of trapezoidal-shaped Characteristic Basis Functions to arrays of electrically interconnected antenna elements", *International Conference on Electromagnetics in Advanced Applications (ICEAA)*, Torino, Sep. 2007.

[21] E. Garcia, C. Delgado, I. G. Diego, and M. F. Catedra, "An iterative solution for electrically large problems combining the Characteristic Basis Function Method and the multilevel fast multipole algorithm," *IEEE Trans. Antennas Propag.*, vol. 56, no. 8, pp. 2363–2371, Aug. 2008.

[22] E. Lucente, and A. Monorchio, "A parallel iteration-free MoM algorithm based on the Characteristic Basis Function Method," *International URSI Commission B - Electromagnetic Theory Symposium*, EMTS, Ottawa, Canada, 2007.

[23] L. Matekovits, V. A. Laza, and G. Vecchi, "Analysis of large complex structures with the synthetic-functions approach", *IEEE Trans. Antennas Propag.*, vol. 55, no. 9, pp. 2509–2521, Sep. 2007.

[24] L. Matekovits, G. Vecchi, G. Dassano, and M. Orefice, "Synthetic function analysis of large printed structures: the solution space sampling approach", *IEEE AP-S International Symposium*, pp. 568–571, Boston, Massachusetts, Jul. 2001.

[25] W. B. Lu, T. J. Cui, Z. G. Qian, X. X. Yin, and W. Hong, "Accurate analysis of large-scale periodic structures using an efficient Sub-Entire-Domain basis function method", *IEEE Trans. Antennas Propag.*, vol. 52, no. 11, pp. 3078–3085, Nov. 2004.

[26] D. J. Bekers, S. J. L. van Eijndhoven, A. A. F. van de Ven, P. p. Borsboom, and A. G. Tijhuis, "Eigencurrent Analysis of Resonant Behavior in Finite Antenna Arrays", *IEEE Trans. Microw. Theory Techn.*, vol. 54, no. 6, pp. 2821–2829, Jun. 2006.

[27] C. Craeye, "A Fast Impedance and Pattern Computation Scheme for Finite Antenna Arrays", *IEEE Trans. Antennas Propag.*, vol. 54, no. 10, pp. 3030–3034, Oct. 2006.

[28] E. Suter, J. R. Mosig, "A subdomain multilevel approach for the efficient MoM analysis of large planar antennas", *Micr. Opt. Technol.* vol. 26, no. 4, pp. 270–277, Aug. 2000.

[29] R. Maaskant, R. Mittra, and A. G. Tijhuis, "Fast solution of multi-scale antenna problems for the square kilometre array (SKA) radio telescope using the Characteristic Basis Function Method (CBFM)," *Applied Computational Electromagnetics Society (ACES) journal*, vol. 24, no. 2, pp. 174–188, Apr. 2009.

[30] M. Arts, M. Ivashina, O. Iupikov, L. Bakker, and R. van den Brink, "Design Considerations of Tapered Slot Phased Array Feeds for Reflec-

tor Antennas," *Proc. European Conference on Antennas and Propag. (EuCAP)*, Barcelona, Spain, Apr., 2010, 1–4.
[31] J. D. Kraus, Ed., *Radio Astronomy, 2nd edition*. Durham, NH: Cygnus-Quasar Books, Nov. 2005.
[32] A. van Ardenne, J. D. Bregman, W. A. van Cappellen, G. W. Kant, J. G bij de Vaate, "Extending the field of view with phased array techniques: results of European SKA research," *Proceedings of the IEEE*, vol. 97, no. 8, pp. 1531–1542, Aug. 2009.

Rob Maaskant received the M.Sc. and Ph.D. degree, both *cum laude*, in Electrical Engineering from the Eindhoven University of Technology, the Netherlands, in 2003 and 2010, respectively. Since 2003, he has been an antenna research engineer at the Netherlands Foundation for Research in Astronomy (ASTRON) where his research is carried out in the framework of the Square Kilometre Array (SKA) radio telescope project. He received the 2nd Best Paper Award ('Best team contribution') at the ESA Antenna Workshop (2008). In 2010, the Netherlands Organization for Scientific Research (NWO) awarded him the Rubicon grant. This grant allows him to perform two years of postdoctoral research at the Chalmers University of Technology, Sweden. Currently, his research interests include the development of numerically efficient integral-equation techniques for large finite array antennas, and the characterization and design of antenna array receiving systems.

Marianna V. Ivashina was born in Ukraine in 1975. She received the combined B.Sc/M.Sc. degree and Ph.D. both in Electrical Engineering from the Sevastopol National Technical University (SNTU), Sevastopol, Ukraine, in 1995 and 2000, respectively. From 2001 to 2004 she was a Postdoctoral Researcher and from 2004 till 2010 an Antenna System Scientist at ASTRON. During this period she has carried out research on an innovative focal plane array (phased array feed) technology for a new generation radio telescope, known as the Square Kilometer Array (SKA). In 2002, she also stayed as a visiting scientist at the European Space Agency (ESA), ESTEC in the Netherlands, where she studied multiple-beam array feeds for the satellite telecommunication system Large Deployable Antenna (LDA) which is being realized by Alenia. She received the URSI Young Scientists Award for GA URSI, Toronto, Canada (1999), APS/IEEE Travel Grant, Davos, Switzerland (2000), the 2nd Best Paper Award ('Best team contribution') at the ESA Antenna Workshop (2008) and the VINNOVA - Marie Curie Actions International Qualification Fellowship (2010) for a joint project with Chalmers University of Technology (Sweden), at which she will be employed for 2 years from January 2011. Her research interests are focal plane arrays, array feeds for reflector antennas, wide-band receiving arrays, and radio astronomy.

Oleg Iupikov received his M.Sc. degree (*cum laude*) in Electrical Engineering from the Sevastopol National Technical University, Ukraine, in 2006. After graduating he has been working for a year at the Radio Engineering Bureau in Sevastopol. Since 2007, he is working toward his Ph.D. degree in the field of phased array feeds and their optimization. He received a Marie Curie visitor grant to perform scientific research at the Netherlands Institute for Radio Astronomy (ASTRON) during the period of 2008-2010.

Elena A. Redkina was born in Ukraine in 1981. She received her M.Sc. degree and Ph.D. both in Electrical Engineering from the Sevastopol National Technical University (SNTU), Sevastopol, Ukraine, in 2003 and 2009, respectively. During 2003-2007, she was an engineer at SNTU, and visited the Netherlands Institute for Radio Astronomy (ASTRON) twice in 2006 in the context of Helena Kluyver's Female Visitor Programme. From 2009 she has been an Assistant Professor at SNTU.

Sreenivas Kasturi (S'98) received the B.Tech degree in Electrical and Electronics Engineering from J.N.T.U. College of Engineering, Hyderabad, India, in 2001, and the M.Sc. and Ph.D. degree in Electrical and Computer Engineering from the University of Massachusetts, Amherst, in 2004 and 2007, respectively. He has presented papers at the annual Antenna Applications Symposium, Allerton Park, and also works as a consulting engineer for antenna array designs. His research interests are in the areas of wideband phased arrays and tapered slot antennas. From 2007, he has been employed at Qualcomm in San Diego, California, where he is a Senior Designer conducting research and developing antenna technologies for cellular and wireless applications.

Daniel H. Schaubert (S'68-M'74-SM'79-F'89) is Professor of Electrical Engineering and Director of the Center for Advanced Sensor and Communication Antennas at the University of Massachusetts. He received the Ph.D. degree in Electrical Engineering from the University of Illinois and worked at the US Army Research Laboratory and the US Food and Drug Administration prior to joining the University of Massachusetts in 1982. His contributions have been mainly in the areas of antenna design and analysis. He has patents for conformal and printed circuit antennas and for wide bandwidth antennas. Several of his antenna designs have been used in military and civilian systems for radars, radiometers and communications, and he has designed low-cost antennas for commercial cellular and local area network products. He directed the design, fabrication and testing of antennas for the Cloud Profiling Radar System, a polarimetric 33-GHz and 95-GHz mobile radar, and the High-Altitude Wind and Rain Profiler, a dual-beam 13-GHz and 35-GHz airborne radar. He led the design efforts for several multioctave scanning array antennas, including the first prototypes for the Thousand Element Array demonstrator of the Square Kilometer Array project.

He was President of the IEEE Antennas and Propagation Society, Associate Editor of the IEEE Transactions on Antennas and Propagation, Secretary-Treasurer of the Society, Newsletter Editor and Membership Chairman. He organizes the annual Antenna Applications Symposium. Professor Schaubert received the John Kraus Antenna Award in 2008, the H. A. Wheeler Prize Applications Paper Award in 1997 and the IEEE Third Millennium Medal.